

Observation of x-ray magnetic scattering in Nd_2CuO_4

J. P. Hill, A. Vigliante, and Doon Gibbs

Department of Physics, Brookhaven National Laboratory, Upton, New York 11973

J. L. Peng and R. L. Greene

Center for Superconductivity Research, Department of Physics, University of Maryland, College Park, Maryland 20742

(Received 16 February 1995)

We report the observation of resonant x-ray magnetic scattering in Nd_2CuO_4 . The experiments were performed by tuning the incident energy to the Nd L_I , L_{II} , and L_{III} absorption edges. The largest count rates, up to 300 counts per second, were obtained at the L_{II} edge. Antiferromagnetic long-range order is seen below $T_{\text{Nd}} = 37$ K. Polarization analysis confirms that the scattering is magnetic in origin and consistent with a dipole excitation, suggesting that the Nd $5d$ bands are polarized.

In order to develop a comprehensive understanding of the high- T_C superconductors, it is useful to study the undoped, parent compounds to characterize the underlying insulating state from which the superconductivity develops. Of particular interest are their magnetic properties, and here common features are seen in La_2CuO_4 , the progenitor of the hole-doped superconductors, and Nd_2CuO_4 and Pr_2CuO_4 , the precursors of electron carrier superconductivity. The magnetic features include (1) three-dimensional (3D) antiferromagnetic long-range order (LRO) of the $\text{Cu}^{2+} S = \frac{1}{2}$ spins, which develops below a Néel temperature in the range $T_N = 250\text{--}325$ K; (2) highly anisotropic Cu^{2+} exchange energies, with the in-plane exchange being at least 4 orders of magnitude larger than the out-of-plane; and (3) 2D inelastic correlations present in the CuO_2 sheets above the Néel transition. The excitations extend to 0.3 eV.¹

There are, however, some important differences between the two classes of materials, including the presence of the rare-earth ions in the electron superconductors. These ions carry localized $4f$ moments, which can themselves order. In contrast, the La^{3+} ions in La_2CuO_4 are nonmagnetic. In this work, we report a study of Nd_2CuO_4 utilizing resonant x-ray magnetic-scattering techniques. The main advantage of these techniques for this problem is the possibility of separating the ordering of the Nd moments from that of the Cu moments by tuning the incident photon energy to a Nd absorption edge. The small spot size and penetration depth of the x rays also obviates the need for large single crystals which are often difficult to obtain. In addition, high spatial resolution offers the possibility of examining mesoscopic length scales. Finally, the energy resolution is inherently poor and therefore essentially all the inelastic fluctuations are integrated. Thus, the quasielastic approximation is exact, even for the high- T_C materials with strongly inelastic fluctuations.

The crystal structure of Nd_2CuO_4 is shown in Fig. 1. The unit cell is tetragonal with room-temperature lattice constants, $a = 3.941$ Å and $c = 12.16$ Å.² The Cu^{2+} moments order in a 3D structure at a Néel temperature of

$T_N = 255$ K.^{2,3} The magnetic structure is noncollinear, with the Cu^{2+} spins aligned antiferromagnetically in the a - b plane and directed along the (100) and (010) directions in successive layers.^{4,5} On further cooling, there are two-spin reorientation transitions.^{2,3,6} At $T = 75$ K, all the Cu^{2+} spins rotate by 90° about the c axis and at $T = 30$ K they rotate back to give the original structure. For temperatures below $T = 30$ K, Matsuda *et al.* found the observed intensities could be modeled by including an ordered moment on the Nd ions.³ The Nd structure is also believed to be noncollinear⁷ and the low-temperature magnetic structure of both sublattices is shown in Fig. 1. One of the main results of the present work is the direct

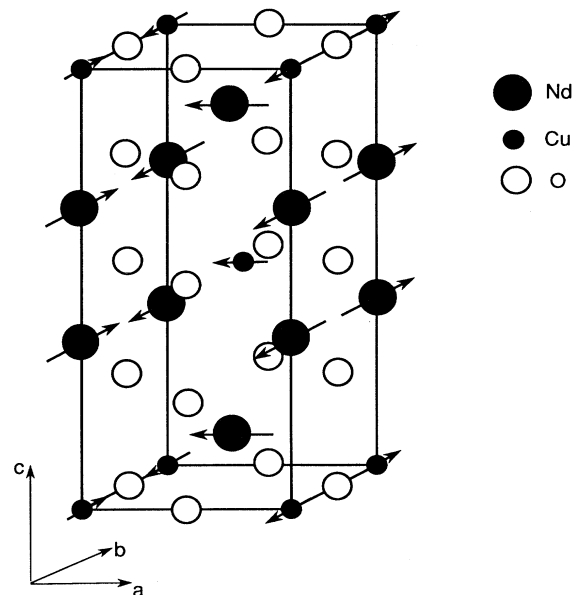


FIG. 1. The crystal and low-temperature magnetic structure of Nd_2CuO_4 . The lattice constants at room temperature are $a = 3.941$ Å and $c = 12.14$ Å.

observation of LRO of the Nd^{3+} moments, confirming this suggestion. At still lower temperatures, there is evidence of further ordering of the Nd moments, at $T \sim 3$ K and $T = 0.8$ K.^{3,8-12}

Resonant x-ray magnetic scattering makes use of large enhancements in the x-ray-scattering cross section which occur on tuning the incident photon energy to an atomic absorption edge. Briefly, the x-ray-scattering cross section per atom may be written as¹³

$$f_n(\mathbf{k}, \mathbf{k}', \hbar\omega) = f_n^{\text{charge}}(\mathbf{Q}) + f_n'(\mathbf{k}, \mathbf{k}', \hbar\omega) + if_n''(\mathbf{k}, \mathbf{k}', \hbar\omega) + f_n^{\text{spin}}(\mathbf{k}, \mathbf{k}', \hbar\omega), \quad (1)$$

where $f_n^{\text{charge}}(\mathbf{Q})$ is the usual Thomson scattering, f_n^{spin} is the part of the cross section which depends explicitly on the electron's spin angular momentum and f_n' and f_n'' are the anomalous scattering terms. \mathbf{k} , \mathbf{k}' , and $\hbar\omega$ are the incident and outgoing wave vectors and photon energy, respectively. $\mathbf{Q} = \mathbf{k}' - \mathbf{k}$. In the vicinity of an atomic absorption edge, the resonant contributions to f_n' and f_n'' become large and may dominate. This scattering can acquire magnetic sensitivity if the particular edge chosen involves the excitation of an electron to a magnetically ordered shell, or alternatively to an exchange-split orbital.^{13,14} Under such conditions, coherent magnetic Bragg diffraction occurs and magnetic correlation lengths and order parameters may be probed in the usual way.¹⁵ In addition, there is a natural element selectivity, since the resonant contributions from a single species tend to dominate. Hence, by tuning to the Nd L edges we are able to probe the ordering of the Nd moments directly, with little expected contribution from the Cu moments.

These experiments were performed on beamline X22C at the National Synchrotron Light Source. The beamline employs a toroidal focusing mirror and a double bounce Ge(111) crystal to deliver a monochromatic beam with a spot size of < 1 mm \times 1 mm at the sample position. For most of these experiments, the beam is scattered vertically onto a Ge(111) flat analyzer crystal, resulting in an energy resolution of ~ 5 eV. For the part of this work involving polarization analysis, a flat Cu(220) crystal, with a mosaic width of 0.044° , was used. The sample was encapsulated in a Be can containing He exchange gas and mounted on the copper cold finger of a closed-cycle He refrigerator. The base temperature of the cryostat was 3.9 K with a temperature stability of $\sim \pm 0.02$ K during the course of a typical scan. Temperatures were measured using a calibrated Si diode.

The samples were grown from a mixture of CuO and Nd_2O_3 which was heated to a temperature of $\sim 1300^\circ\text{C}$ for several hours and then cooled slowly to room temperature. This procedure resulted in the formation of free standing crystal platelets of approximate thickness 0.1 mm with a surface normal along the c axis. For this work, a crystal of size $17 \times 4 \times 0.1$ mm³ and a mosaic width of 0.014° full width at half maximum was chosen.

It was mounted such that Bragg peaks of type (h, h, l) lay in the scattering plane. As noted above, antiferromagnetic order develops with a propagation vector along the diagonals of the CuO square lattice. Reflections of the type (h, h, l) with h, l integers arise from charge scattering, while $(h/2, h/2, l)$ reflections arise from magnetic scattering. The crystal morphology and reflection geometry restrict the accessible region of reciprocal space to reflections close to the $(00L)$ specular direction. The $(0.5, 0.5, 8)$ magnetic peak chosen for this work was the most intense of the easily accessible magnetic reflections.

The central result of this paper is the observation of magnetic scattering when the incident photon energy was tuned to the Nd L edges at 7126 eV (L_I), 6722 eV (L_{II}), and 6208 eV (L_{III}), for temperatures below $T = 37$ K. Significant enhancements of the magnetic scattering from the Nd^{3+} ions were observed. The intensities of the charge and magnetic Bragg peaks as a function of the incident energy, through the L_{II} edge, are shown in Fig. 2. These data were taken at $T = 4$ K. The (118) charge peak shows the characteristic dip and recovery expected from the interference of the anomalous scattering terms in the cross section [Fig. 2(a)]. The intensity of the $(0.5, 0.5, 8)$, however, exhibits a dramatic enhancement corresponding to x-ray resonant exchange scattering [Fig. 2(b)]. The maximum count rate obtained at the L_{II} edge was 300 counts per second for a storage ring current of 200 mA at $T = 4$ K.¹⁶ The maximum occurred at 6725 eV. This is, to within calibration errors, equal to the nominal value of the L_{II} edge, 6722 eV. The line shape exhibits a slight asymmetry, with a tail at lower energies. This sort of feature has previously been observed in Ho, where it is believed to arise from interference between the non-resonant and resonant magnetic scattering.¹⁷ The data obtained on tuning through the L_{III} absorption edge at $T = 4$ K are shown in Fig. 3. In this case, the enhancement of the magnetic signal was smaller, and a maximum count rate of 3 counts/s at 6215 eV was obtained. A smaller enhancement again was observed at the L_I edge. A count rate of ~ 1 count/s was realized at 7128 eV.

The relative strengths of the different resonances are not fully understood. One-electron calculations of the resonant enhancement in the spherical approximation predict that the L_{II} and L_{III} resonances of Nd should be of similar magnitude.¹⁴ These calculations assume atomic wave functions for the $4f$ and $5d$ orbitals and ignore the perturbing influence of the core hole during the excitation process. For dipole transitions, the L_{II} resonance couples $2p_{1/2}$ and $5d$ states and the L_{III} resonance couples $2p_{3/2}$ to $5d$ states. For quadrupole excitations, the intermediate state is an unoccupied $4f$ orbital. We note that recent studies appear systematic in the relative enhancements at the L_{II} and L_{III} edges. In the heavy rare earths (greater than half filling of the $4f$ shell), Tb,¹⁸ Ho,¹⁷ Er,¹⁹ and Tm,²⁰ the L_{III} edge exhibits the larger enhancement. For the light rare earths (less than half filling), Nd,²¹ and Pr,²² the L_{II} resonance is greater. It remains an open question as to why this is so. Studies of Gd (exactly half filled $4f$) may be illuminating in this regard. A recent study of a random Ho-Pr alloy showed

that the L_{III} resonance is the larger for the Ho edges and the L_{II} is more intense for the Pr.²² This result suggests that the relative strengths of the resonances may not be due to the influence of crystal fields or other solid-state effects, since it is believed that the composition of the Ho-Pr samples was uniform and that the crystalline environment of the two species was similar.

In order to verify that the scattering at (0.5,0.5,8) is indeed of magnetic origin, we have carried out polarization analysis of the charge and magnetic scattering using an instrument described previously.²³ Briefly, an analyzer crystal is chosen such that its Bragg angle, θ_A , is as close as possible to 45° . If it is set to scatter in the

(vertical) scattering plane, the horizontal, σ -polarized, component will be passed. Conversely, if it is rotated by 90° about the scattered beam, to diffract horizontally, then the vertical, or π -polarized component is detected. The reflection chosen in this case was the $\text{Cu}(220)$, with $\theta_A = 46.27^\circ$ at the Nd L_{II} edge. The deviation from the ideal value results in a negligible "leakage" from one channel to the other.

Thomson scattering is not expected to rotate the polarization of the incident photon. At the bending magnet source, X22C, where the incident beam is 95% horizontally polarized, charge scattering will produce a largely σ -polarized scattered beam. This is illustrated in Fig. 4(a) which shows the σ - and π -polarized components (open and closed circles, respectively) obtained at the (118) reflection. The scattering is predominately σ polarized in the ratio 300:1. This is consistent with charge scattering with 95% incident σ polarization, a Bragg angle of $2\theta_B = 87.83^\circ$ and a small "leakage." At the (0.5,0.5,8)

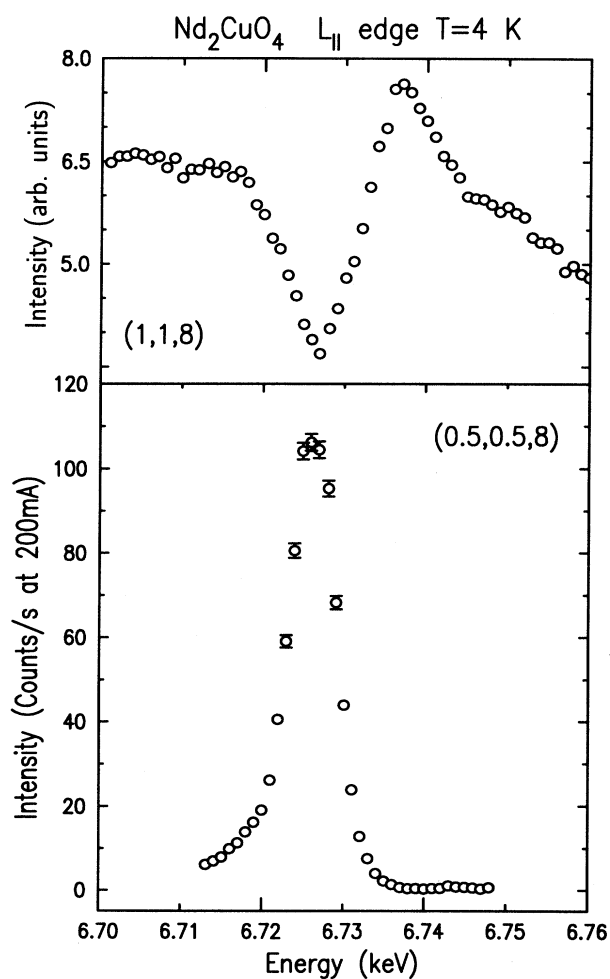


FIG. 2. The Bragg peak intensities recorded as the incident photon energy is tuned through the Nd L_{II} edge at $T=4$ K. (a) The (1,1,8) charge Bragg peak. The dip and recovery results from interference between the anomalous scattering terms in the cross section. (b) The (0.5,0.5,8) magnetic Bragg peak. There is a large enhancement in the coherent Bragg scattering from the Nd ions as the absorption edge is reached.

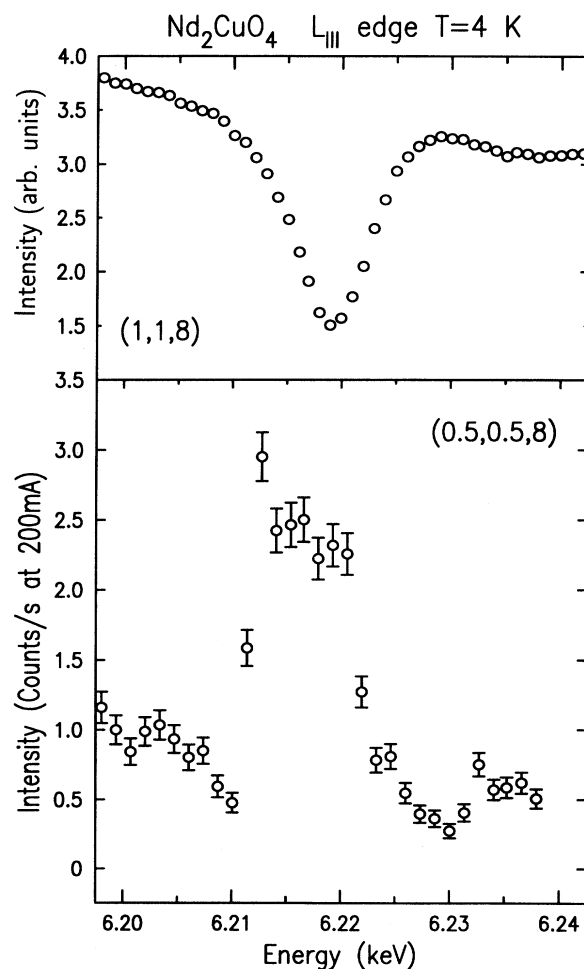


FIG. 3. As Fig. 2, with the incident photon energy tuned through the L_{III} edge. The magnetic enhancement is significantly smaller at this edge. $T=4$ K.

magnetic peak the situation is reversed, as shown in Fig. 4(b). These data were taken with an incident photon energy of 6725 eV. Here the π component dominates the scattered beam, i.e., the scattering has rotated the incident polarization. This is characteristic of magnetic scattering, and together with the energy dependence of Fig. 2, establishes that the (0.5,0.5,8) Bragg peak is magnetic. The possibility that it is a superlattice peak arising from a structural phase transition, such as occurs in La_2CuO_4 (Ref. 24) is thus ruled out. Polarization analysis was not attempted at either the L_I or L_{III} edges.

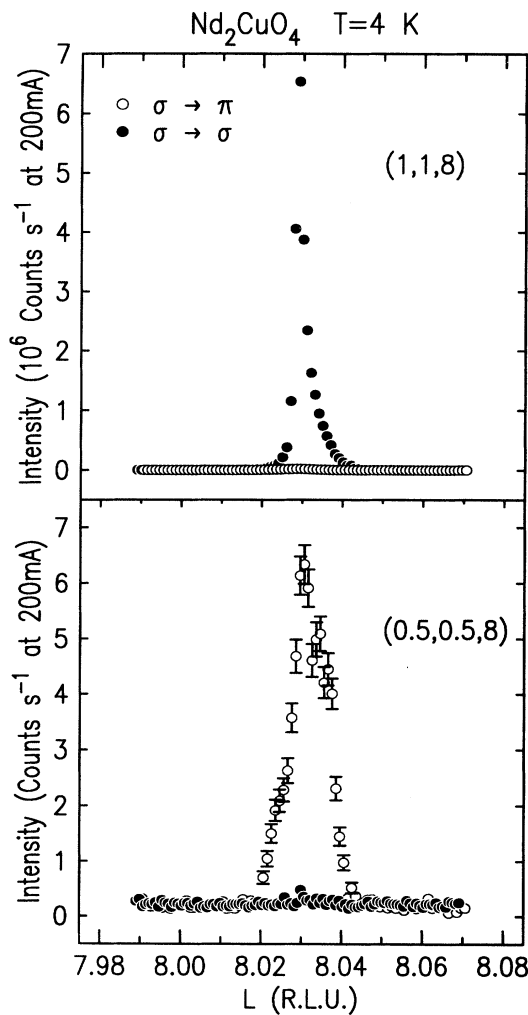


FIG. 4. Polarization analysis at the charge and magnetic Bragg peaks at $T=4$ K. The closed circles represent $\sigma \rightarrow \sigma$ scattering, that is scattering which leaves the incident polarization unchanged. The open circles are $\sigma \rightarrow \pi$ scattering, that is scattering for which the polarization of the scattered beam has been rotated by 90° with respect to the incident. (a) The charge peak (1,1,8). (b) The magnetic peak (0.5,0.5,8). The charge scattering is predominately $\sigma \rightarrow \sigma$ and the magnetic scattering is predominately $\sigma \rightarrow \pi$.

The polarization dependence of the resonant cross section may be calculated^{13,15} for both dipole and quadrupole excitations at each L edge. For peaks of the type $(h/2, h/2, l)$ and the spin structure of Fig. 1, dipole excitations give no $\sigma \rightarrow \sigma$ scattering. The scattering expected is almost entirely $\sigma \rightarrow \pi$. For quadrupole scattering, however, the $\sigma \rightarrow \sigma$ channel is no longer forbidden. The fact that the σ channel is zero to within our limits of detection (counting for 220 s on a background of 0.2 counts per second), leads us to conclude that the scattering observed at the L_{II} edge results from dipole transitions. This is consistent with previous work on Ho, for which the dipole scattering was a factor of 5 larger than the quadrupole.^{17,25} [In the earlier work, it was also found that the quadrupole excitation occurred at a slightly lower energy (≈ 3 eV).] If the scattering is dipole, then there must be a net polarization of the Nd $5d$ bands in addition to that of the $4f$ moments. Such a polarization mediates an indirect exchange interaction among the Nd moments. This Nd^{3+} - Nd^{3+} interaction will give rise to spontaneous ordering of the Nd spin system, at some sufficiently low temperature $T_{\text{Nd-Nd}}$. In the presence of the Cu ordering field, this transition is smeared and is signaled by a rapid increase in the Nd ordered moment at $T_{\text{Nd-Nd}}$. Such an increase and other evidence of spontaneous ordering has been seen around $T \leq 3$ K (Refs. 3 and 8–12) and in our own data, as we discuss shortly. In addition, the polarization of the Nd d bands mediates the Nd^{3+} - Cu^{2+} indirect exchange interaction.

In Fig. 5, we present scans through the (0.5,0.5,8) magnetic Bragg peak at $T=4$ K. These data were taken with a flat Ge(111) analyzer. The solid lines represent fits to Lorentzian squared functions, which were used to conveniently parametrize the data. Unfortunately, it was not possible to deconvolve the experimental resolution from the data because of a lack of detailed knowledge of the resolution function at the momentum transfer of the magnetic peak, $q=4.291 \text{ \AA}^{-1}$. This problem is exacer-

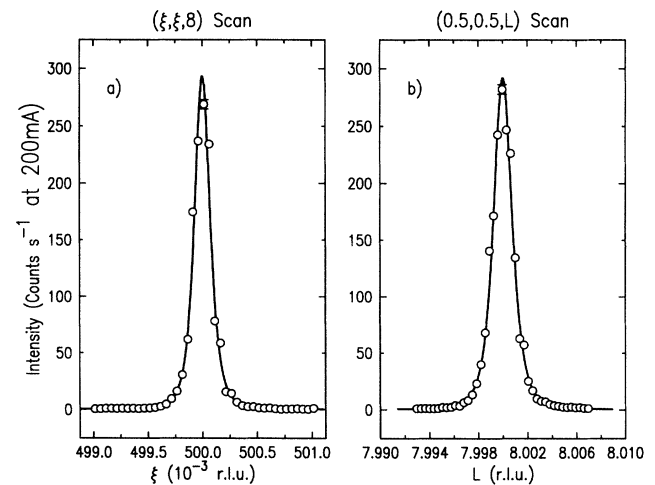


FIG. 5. Representative scans through the magnetic Bragg peak (0.5,0.5,8) at $T=4$ K. (a) In-plane scan. (b) Scan along the c axis. Solid lines are fits to Lorentzian squared line shapes.

bated because the spectrometer is far from the nondispersive condition, $q = 1.924 \text{ \AA}^{-1}$. Nevertheless, we are able to make statements concerning lower bounds for the correlation lengths, by assuming a δ -function resolution. With such a conservative assumption, we find $\xi_{aa} \geq 2300 \pm 100 \text{ \AA}$ and $\xi_c \geq 7500 \pm 400 \text{ \AA}$, where ξ_{aa} is the in-plane correlation length along the diagonals of the CuO sheet and ξ_c is the out-of-plane correlation length, along the c axis. In fact, the (0.5,0.5,8) magnetic Bragg peak was found to be narrower than the (118) charge Bragg peak. We conclude that it is resolution limited and that the Nd moments are aligned antiferromagnetically in a long-range ordered state.

The magnetic peak intensity is plotted as a function of temperature in Fig. 6. The data were taken on warming from the base temperature, avoiding the hysteresis effects discussed in Ref. 3. The intensity is seen initially to fall rapidly, up to $T \sim 10 \text{ K}$. Above $T = 10 \text{ K}$, the intensity continues to decrease, although more slowly, and as shown in the inset to Fig. 6, it passed below the level of detectability at $T_{\text{Nd}} = 37 \pm 2 \text{ K}$. The large error bars arise from a sensor calibration error discovered subsequent to the completion of the experiment. The width of the magnetic peak is constant for all temperatures, that is, the Nd LRO is retained at least up to $T = 37 \text{ K}$.

The origin of the Nd ordered moment lies in the Nd^{3+} - Cu^{2+} exchange coupling. Although this is zero for nearest-neighbor interactions because of the antiferromagnetic order and the tetragonal symmetry, it is appreciable for next-nearest-neighbor Nd^{3+} - Cu^{2+} spins. In a mean-field picture,³ the size of the induced Nd moment will be proportional to the ordered Cu moment times the interaction strength. The constant of proportionality is just the single-ion paramagnetic susceptibility of the Nd^{3+} ion within the a - b plane. In this picture, there is an ordered Nd^{3+} moment for all temperatures below $T_N = 255 \text{ K}$. However, the size of that moment is controlled by the susceptibility which only becomes appre-

ciable around $T = 30 \text{ K}$.¹² This explains the disappearance of the signal at $T_{\text{Nd}} = 37 \text{ K}$ and is in agreement with the interpretation of the neutron-scattering data.^{2,3,8} In Ref. 3, T_{Nd} is identified with the second spin reorientation transition, thus suggesting that the origin of these transitions lies in the competing Nd^{3+} - Cu^{2+} and Cu^{2+} - Cu^{2+} interactions. It is not possible from our current data set to comment on this possibility.

The steep rise in scattered intensity at low temperatures represents a rapid increase in the Nd ordered moment. It seems likely that this is the signature of the approaching Nd ordering transition at $T \leq 3 \text{ K}$. As discussed above, this is the temperature at which the Nd^{3+} - Nd^{3+} interactions alone would be sufficient to give rise to LRO of the Nd moments. This transition has been found to be broad in the pure material and sharp, with $T_N = 1.5 \text{ K}$, in a Ce-doped superconducting sample.⁸

In summary, we have observed LRO of the Nd moments in Nd_2CuO_4 with resonant x-ray magnetic scattering. The largest enhancement was obtained at the L_{II} edge. The polarization dependence of the magnetic scattering is consistent with a dipole excitation into a polarized $5d$ conduction band state. While symmetry arguments require the Nd moments to order for all temperatures below the 3D ordering temperature of the Cu spins, $T_N = 255 \text{ K}$, the ordered Nd moment only becomes measurable at $T_{\text{Nd}} = 37 \text{ K}$. At low temperatures the ordered moment is seen to rise rapidly. These results confirm earlier interpretations of neutron-scattering data.³ The significance of this work, however, lies in the successful application of x-ray magnetic scattering to the high- T_C problem. While these measurements are sensitive to the Nd moments, which are presumed to participate in the magnetism only parasitically, the availability of high-quality crystals and third generation synchrotron sources suggests that it will be possible to observe the Cu moments directly in the near future. Such experiments will exploit the relatively poor energy resolution of the x-ray-scattering technique to measure the energy integrated response, i.e., the instantaneous spin-spin correlation function. More immediately, studies of doped, superconducting samples, would elucidate the behavior of the Nd moments in the superconducting state. Preliminary experiments on 15% Ce-doped samples, both annealed and as-grown, showed no evidence of x-ray magnetic scattering. However, these samples exhibited significantly larger mosaic widths than those in the present work. Future work on higher-quality samples is planned.

We thank W. J. Nuttall, W. G. Stirling, and D. M. Zehner for useful discussions. In addition, we are grateful to D. M. Zehner for the loan of the $\text{Cu}(220)$ crystal and J. Bohr for the loan of his polarization analyzer. The work at Brookhaven National Laboratory was carried out under Contract No. DE-AC02-76CH00016, Division of Materials Science, U.S. Department of Energy. The work at the University of Maryland was supported by the National Science Foundation under Grant No. DMR 9209668.

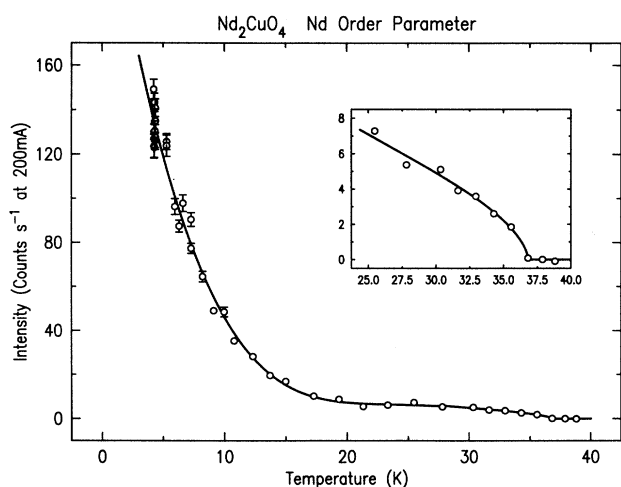


FIG. 6. Magnetic peak intensity as a function of temperature. The inset shows the intensity reaching zero at $T_{\text{Nd}} = 37 \text{ K}$. The solid line is a guide to the eye.

- ¹S. M. Hayden, G. Aeppli, R. Osborn, A. D. Taylor, T. G. Perring, S-W. Cheong, and Z. Fisk, *Phys. Rev. Lett.* **67**, 3622 (1991).
- ²Y. Endoh, M. Matsuda, K. Yamada, K. Kakurai, Y. Hidaka, G. Shirane, and R. J. Birgeneau, *Phys. Rev. B* **40**, 7023 (1989).
- ³M. Matsuda, K. Yamada, K. Kakurai, H. Kadowaki, T. R. Thurston, Y. Endoh, Y. Hidaka, R. J. Birgeneau, M. A. Kastner, P. M. Gehring, A. H. Moudden, and G. Shirane, *Phys. Rev. B* **42**, 10 098 (1990).
- ⁴S. Skanthakumar, J. W. Lynn, J. L. Peng, and Z. Y. Li, *Phys. Rev. B* **47**, 6173 (1993).
- ⁵S. Skanthakumar, J. W. Lynn, J. L. Peng, and Z. Y. Li, *J. Appl. Phys.* **73**, 6326 (1993).
- ⁶G. M. Luke, L. P. Le, B. J. Sternlieb, Y. J. Uemura, J. H. Brewer, R. Kadono, R. F. Kiefl, S. R. Kreitzman, T. M. Riseman, C. E. Stronach, M. R. Davis, S. Uchida, H. Takagi, Y. Tokura, Y. Hidaka, T. Murakami, J. Gopalakrishnan, A. W. Sleight, M. A. Subramanian, E. A. Early, J. T. Markert, M. B. Maple, and C. L. Seaman, *Phys. Rev. B* **42**, 7981 (1990).
- ⁷A. S. Cherny, E. N. Khats'ko, G. Chouteau, J. M. Louis, A. A. Stepanov, P. Wyder, S. N. Barilo, and D. I. Zhigunov, *Phys. Rev. B* **45**, 12 600 (1992).
- ⁸J. W. Lynn, I. W. Sumarlin, S. Skanthakumar, W-H. Li, R. N. Shelton, J. L. Peng, Z. Fis, and S-W. Cheong, *Phys. Rev. B* **41**, 2569 (1990).
- ⁹S. Skanthakumar, H. Zhang, T. W. Clinton, W-H. Li, J. W. Lynn, Z. Fisk, and S-W. Cheong, *Physica C* **160**, 124 (1989).
- ¹⁰S. Ghamaty, B. W. Lee, J. T. Markert, E. A. Early, T. J. Bjornholm, G. L. Seaman, and M. B. Maple, *Physica C* **160**, 217 (1989).
- ¹¹J. T. Markert, E. A. Early, T. Bjornholm, S. Ghamaty, B. W. Lee, J. J. Neumeier, R. D. Price, G. L. Seaman, and M. B. Maple, *Physica C* **158**, 178 (1989).
- ¹²M. F. Hundley, J. D. Thompson, S. W. Cheong, Z. Fisk, and S. B. Oseroff, *Physica C* **158**, 109 (1989).
- ¹³J. P. Hannon, G. T. Trammel, M. Blume, and D. Gibbs, *Phys. Rev. Lett.* **61**, 1245 (1988).
- ¹⁴M. D. Hamrick, Ph.D. thesis, Rice University, 1994.
- ¹⁵J. P. Hill and D. F. McMorrow (unpublished).
- ¹⁶The data of Figs. 2 and 6, which show a maximum count rate of ~ 100 counts/s are from an initial run. Subsequent runs utilized a different point on the sample, resulting in higher count rates, see Fig. 5. The data of Fig. 4 are also from the second run. There were no other observed differences in the two runs.
- ¹⁷D. Gibbs, G. Grubel, D. R. Harshmann, E. D. Isaacs, D. B. McWhan, D. Mills, and C. Vettier, *Phys. Rev. B* **43**, 5663 (1991).
- ¹⁸R. R. Chistyakov, H. Kawata, K. Mori, Y. Koyama, K. Namikawa, V. A. Belyakov, and S. N. Nikitin (unpublished).
- ¹⁹D. Gibbs *et al.* (unpublished).
- ²⁰J. Bohr, D. Gibbs, and K. Huang, *Phys. Rev. B* **42**, 4332 (1990).
- ²¹D. Watson, E. M. Forgan, W. J. Nuttall, W. G. Stirling, and D. Fort (unpublished).
- ²²A. Vigliante, G. Helegesen, J. P. Hill, D. F. McMorrow, R. A. Cowley, and D. Gibbs (unpublished).
- ²³D. Gibbs, M. Blume, D. R. Harshman, and D. B. McWhan, *Rev. Sci. Instrum.* **60**, 1655 (1989).
- ²⁴K. Yamada, M. Matsuda, Y. Endoh, B. Keimer, R. J. Birgeneau, S. Onodera, J. Mizusaki, T. Matsuura, and G. Shirane, *Phys. Rev. B* **39**, 2336 (1989).
- ²⁵G. Helgesen, J. P. Hill, T. R. Thurston, D. Gibbs, J. Kwo, and M. Hong, *Phys. Rev. B* **50**, 2990 (1994).